

# Inviscid coalescence of drops

By L. DUCHEMIN<sup>1</sup>, J. EGGERS<sup>2</sup> AND C. JOSSERAND<sup>3</sup>

<sup>1</sup>Department of Mathematics, Imperial College of Science, Technology and Medicine,  
180 Queen's Gate, London, SW7 2BZ, UK

<sup>2</sup>Fachbereich Physik, Universität Gesamthochschule Essen, 45117 Essen, Germany

<sup>3</sup>Laboratoire de Modélisation en Mécanique, 8, rue du Capitaine Scott, 75015 Paris, France

(Received 13 December 2002 and in revised form 19 February 2003)

We study the coalescence of two drops of an ideal fluid driven by surface tension. The velocity of approach is taken to be zero and the dynamical effect of the outer fluid (usually air) is neglected. Our approximation is expected to be valid on scales larger than  $\ell_v = \rho v^2 / \sigma$ , which is 10 nm for water. Using a high-precision boundary integral method, we show that the walls of the thin retracting sheet of air between the drops reconnect in finite time to form a toroidal enclosure. After the initial reconnection, retraction starts again, leading to a rapid sequence of enclosures. Averaging over the discrete events, we find the minimum radius of the liquid bridge connecting the two drops to scale like  $r_b \propto t^{1/2}$ .

---

## 1. Introduction

Drop coalescence arises in many different contexts, and is crucial to our understanding of free surface flows (Eggers 1997). Examples are printing applications (Chaudhary & Maxworthy 1980; Wallace 2001), drop impact on a fluid surface (Oguz & Prosperetti 1990), and the coarsening of drop clouds and dispersions (MacPhee *et al.* 2002; Jury *et al.* 1999; Verdier 2000). After the two surfaces have merged on a microscopic scale, surface tension drives an extremely rapid motion, usually impossible to resolve in either experiment (Bradley & Stow 1978; Menchaca-Rocha *et al.* 2001) or simulation (Lafaurie *et al.* 1994). Thus theory is needed to investigate a possible dependence on initial conditions, development of small-scale structures during merging, and to estimate the typical time required for merging.

A large body of work exists on this problem in the case where viscosity is dominant and the motion is described by Stokes' equation. In the absence of an outer phase this is known as the 'viscous sintering problem' (Frenkel 1945; Hopper 1993; Martinez-Herrera & Derby 1995); the inclusion of an outer phase is important for many problems governing the coarsening of dispersion (Nikolayev, Beysens & Guenoun 1996; Verdier 2000). For the two-dimensional problem (i.e. for the merging of cylinders) *exact* solutions exist (Hopper 1990; Richardson 1992; Crowdy 2002, 2003), which were shown (Eggers, Lister & Stone 1999) to be asymptotically equivalent to their three-dimensional counterparts. The presence of an outer fluid leads to the formation of a toroidal bubble during merging (Eggers *et al.* 1999), significantly modifying the dynamics.

Figure 1 shows two equal drops of radius  $R$  connected by a liquid bridge of radius  $r_b$ , which is rapidly being pulled up by surface tension. The local Reynolds number of this flow can be estimated as  $Re = \sigma r_b / (\rho v^2)$ , where  $\sigma$  is the surface tension,  $\rho$  the density, and  $v$  the kinematic viscosity. Thus, regardless of the value of the

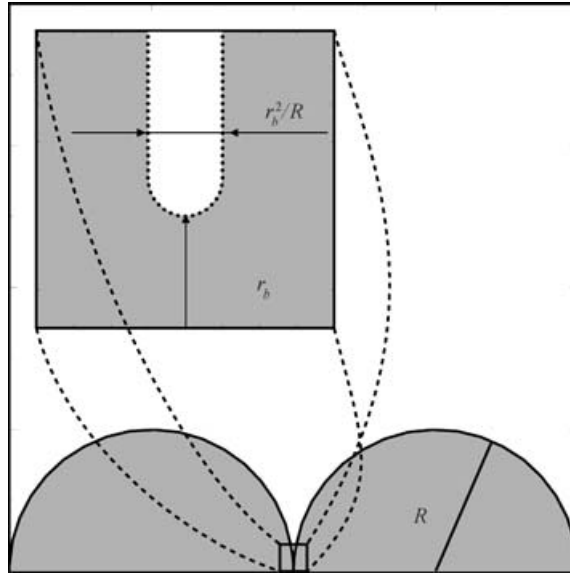


FIGURE 1. Initial condition. Two drops touching at a point are joined by a liquid bridge of radius  $r_b$ . The inset shows the width of the gap just above the meniscus to be  $w = r_b^2/R$ . The gap's walls are nearly straight on the scale of  $w$ .

viscosity, the Reynolds number is always small in the initial phases of the merging, which is equivalent to requiring that  $r_b \ll \ell_v$ , where  $\ell_v = \nu^2 \rho / \sigma$  is the viscous length scale. However,  $\ell_v$  is often very small (140 Å for water, and 4 Å for mercury (Eggers 1997)), so  $r_b \gg \ell_v$  for a large part of the evolution, and inviscid theory can be applied. Thus for a wide range of practical problems the almost inviscid regime, which is the topic of this letter, is the most relevant. Typically, the viscous regime will serve as an inner layer that defines the initial condition for the inviscid problem that we are interested in. In general, we do not have to consider the initial process of reconnection (Amarouchene, Cristobal & Kellay 2001), which for clean fluids is expected to take place over a microscopically small area.

In the case of a head-on collision of two drops with relative velocity  $V$ , considered in Oguz & Prosperetti (1989), a purely geometrical consideration predicts  $r_b \approx \sqrt{VRt}$  for two overlapping circles. The corresponding speed of merging is of the same order as the surface-tension-driven merging to be described below, so  $V$  has thus to be taken into account. However, we will restrict ourselves here to the case where the velocity of approach is vanishingly small, a condition that is easily realizable experimentally (Menchaca-Rocha *et al.* 2001). We also do not treat the dynamical effect of an outer fluid like air, which might become important as the lubrication layer between the approaching drops becomes very thin (Eggers *et al.* 1999; Yiantsos & Davis 1991). However, this approximation is consistent with the assumption of a small velocity of approach.

## 2. Initial conditions and scaling laws

We consider two identical drops of radius  $R$  touching at a point where a thin liquid bridge of size  $r_b$  connects the two drops initially (cf. figure 1). The general problem

of drops of different radii only changes a prefactor in the gap width between the drops (Eggers 1998). For the inviscid dynamics considered here, all parameters of the problem can be scaled out by writing the time and space coordinates in units of  $\sqrt{\rho R^3/\sigma}$  and  $R$ , respectively. Assuming that the vorticity generated by the initial viscous motion can be neglected, and using incompressibility, the velocity potential  $\varphi$  obeys

$$\Delta\varphi = 0. \quad (2.1)$$

The boundary condition on the free surface amounts to a balance between surface tension and Bernoulli pressures (Oguz & Prosperetti 1989):

$$\frac{\partial\varphi}{\partial t} + \frac{1}{2}(\nabla\varphi)^2 - \kappa = 0, \quad (2.2)$$

where  $\kappa$  is the mean curvature of the interface.

We have to solve (2.1), (2.2) with the initial condition shown in figure 1, for  $R = 1$  and assuming that the bridge radius  $r_b$  is initially very small (typically  $10^{-5}$  in our numerical simulations). Let  $z$  be the axis of symmetry, and let the surface of the drops be described by  $r = h(z)$ . Away from the point of contact at  $z = 0$ , but for  $h \ll 1$ , the surface has the form  $h(z) = (2z)^{1/2}$  and  $h(z) = (-2z)^{1/2}$  for  $z > 0$  and  $z < 0$ , respectively. The width of the gap at a height  $r$  is thus

$$w = r^2 \quad (r_b \ll r \ll 1) \quad (2.3)$$

and since  $\partial w/\partial r \ll 1$ , the walls are nearly parallel. Thus the meniscus, which owing to radial symmetry is located along a ring of radius  $r_b$ , is being pulled straight up by a force  $2\sigma$  per unit length.

Assuming that the profile in region (2.3) matches onto the bridge on the scale  $r \approx r_b$ , the curvature at the meniscus can be estimated as  $\kappa_b \approx r_b^{-2}$ , much larger than the axial curvature  $r_b^{-1}$  of the liquid bridge. Notice that the right-hand side of this estimate must be multiplied by the drop radius  $R$  to make it dimensionally consistent, but we will use non-dimensional variables throughout this paper. Thus, as already argued in Eggers *et al.* (1999), the axial curvature can be neglected for  $r_b \ll 1$  and the problem becomes effectively two-dimensional, equivalent to the merging of two fluid cylinders. Thus a model problem (Oguz & Prosperetti 1989; Eggers 1998) for the initial motion of the meniscus is that of the two-dimensional, straight slot shown in the inset of figure 1. The eventual widening of the gap can be neglected on the scale of the gap width  $w$ .

The results of our computations for the full three-dimensional problem, to be explained in more detail below, are shown in figure 2. As the meniscus retracts, the rapid fluid flow past the sides of the gap creates an under-pressure as described by Bernoulli's equation (2.2), which in turn causes the end to expand into a bubble. As the bubble increases in size, capillary waves are excited in its wake, with amplitude roughly proportional to the bubble radius. Thus after the amplitude of the capillary wave has grown to the half width of the slot  $w/2$ , its two sides touch and reconnect at a time  $\tau_c$ . Since the width is the only length scale in the problem, it follows that the total length  $r_c$  that the meniscus has retracted up to the point of reconnection is proportional to  $w$ , while the time  $\tau_c$  required scales like  $w^{3/2}$ . We thus have

$$r_c = r_0 w, \quad \tau_c = \tau_0 w^{3/2}, \quad (2.4)$$

where  $r_0, \tau_0$  are constants to be determined numerically. Below we find  $r_0 = 10$ ,  $\tau_0 = 7.6$ .

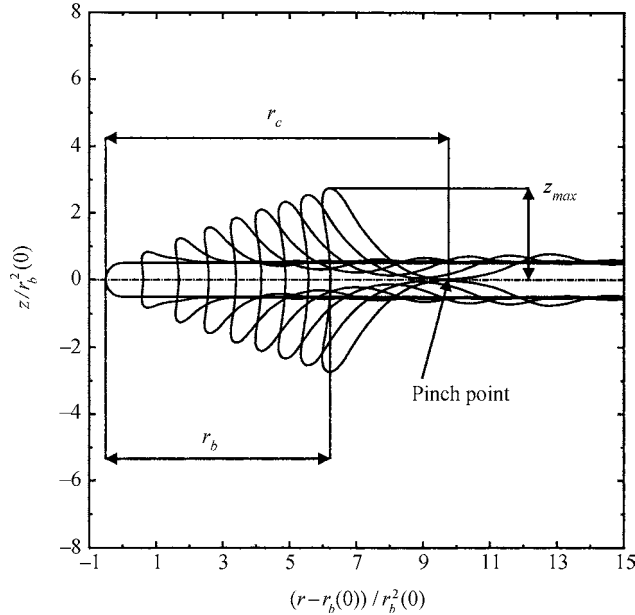


FIGURE 2. A sequence of profiles showing the retraction of the initial meniscus for  $r_b(0) = 10^{-5}$ . At a time  $\tau_c = \tau_0 w^{3/2} = 7.6 w^{3/2}$  the walls of the gap touch and the minimum radius  $z_{min}$  goes to zero. The distance of this point from the initial tip of the meniscus is  $r_c = r_0 w = 10w$ .

After the two sides of the gap have reconnected, this new initial condition looks very similar to the original one, except for a non-trivial velocity field that remains. But since most of the resistance to the motion before reconnection is due to the large bubble that was left behind, this velocity can be neglected relative to the velocity to be generated at the next stage of the motion (more detailed estimates are given below). This means that at each step the same motion is repeated, but with a slightly larger radius  $r_b$ . The distance  $r_b^{n+1} - r_b^n$  between two steps corresponds to the length  $r_c$  that the meniscus has retracted at the time of the next reconnection event, as given by (2.4). At the  $n$ -th step we can thus write, analogous to Eggers (1998),

$$r_b^{n+1} - r_b^n = r_c = r_0 (r_b^n)^2,$$

and for the times  $t_n$  of successive reconnection events:

$$t_{n+1} - t_n = \tau_0 (r_b^n)^3.$$

For very small initial  $r_b$  reconnection occurs in rapid succession, with small relative change of the variables. We can thus write  $r_b$  as a smooth function of  $t$ , obeying the differential equation

$$\frac{dr_b}{dt} \approx \frac{r_0}{\tau_0} \frac{1}{r_b}, \quad (2.5)$$

which gives, after integration,

$$r_b \approx \sqrt{\frac{2r_0}{\tau_0}} t^{1/2}. \quad (2.6)$$

The scaling law (2.6) is the central result of the present paper. Eventually, when  $r_b$  is of the same order as the drop radius, the widening of the channel overcomes

the growth of capillary waves, and the enclosure of bubbles stops. This is when the time scale of retraction  $\tau \approx r_b^2 \tau_0 / (2r_0)$  is shorter than  $\tau_c \approx \tau_0 r_b^3$  characterizing reconnection. Thus reconnection will cease when  $r_b \gtrsim 1/(2r_0) = 0.05$ . We have determined numerically that no more voids are entrapped for  $r_b > 0.035$ , in good agreement with our theoretical estimate. Below we present detailed numerical tests of the scaling predictions, and investigate further the crucial stage of bubble growth, from which we are able to extract the numerical constants  $r_0, \tau_0$ .

### 3. Boundary integral method

If the flow can be considered potential and incompressible, the use of a boundary integral method is advantageous, since the velocity field can be calculated from the interface shape. Thus one only needs to keep track of the interface, represented by a one-dimensional curve, and grid refinement can be done very efficiently. The majority of these boundary integral methods require smoothing of the surface, in order to avoid short-wavelength instabilities. The method briefly presented here does not require any explicit smoothing, except for a redistribution of the points around the tip at every time step. This redistribution can act as a smoothing, but no damping of instabilities, such as an artificial surface viscosity, has been used.

The dipole formulation used here is very close to the one described by Baker, Meiron & Orszag (1980), but it needs to be refined to be able to resolve the very disparate scales of the drops and of the highly curved region close to the meniscus. At a given time step, we expect the velocity potential  $\varphi$  to be known, from which we calculate the normal and the tangential velocity of the surface. This velocity is then used to advect the surface, and to advance  $\varphi$  using Bernoulli's equation (2.2). The tangential velocity is calculated directly by differentiating with respect to the arclength along the interface:

$$u_t = \frac{\partial \varphi}{\partial s}. \quad (3.1)$$

To compute the normal component, we use the vector potential  $\mathbf{A}$  of the velocity field,  $\mathbf{u} = \nabla \times \mathbf{A}$ :

$$\mathbf{u}_n = \frac{1}{r} \frac{\partial r A_\theta}{\partial s}. \quad (3.2)$$

Following Barker *et al.* (1980), we first compute the dipole density  $\mu$  from

$$\varphi(M) = \mu(M) + \frac{1}{4\pi} \int_S (\mu(M) - \mu(M')) \frac{\partial}{\partial n} \left( \frac{1}{\lambda} \right) dS', \quad (3.3)$$

where  $\lambda$  is the distance between points  $M$  and  $M'$  on the surface. The appearance of  $\mu(M)$  in the integrand serves to subtract the singularity of the normal derivative. Once  $\mu$  is known, it can be used to calculate the vector potential:

$$\mathbf{A}(M) = \frac{1}{4\pi} \int_S (\mu(M') - \mu(M)) \mathbf{n} \times \nabla_s \left( \frac{1}{\lambda} \right) dS'. \quad (3.4)$$

Equation (3.3) was solved for  $\mu$  by matrix inversion, then (3.4) was used to calculate  $\mathbf{A}(M)$ . A simple trapezoidal rule was used to convert the equations into linear systems, which were then solved by LU decomposition. In order to compute the curvature of the surface and the tangential derivatives in (3.1), (3.2), we re-parameterized the integrals by introducing a new integration variable  $\zeta$ , which equals  $i$  at grid point  $i$ . This avoids instabilities in the cubic spline interpolation that would otherwise be

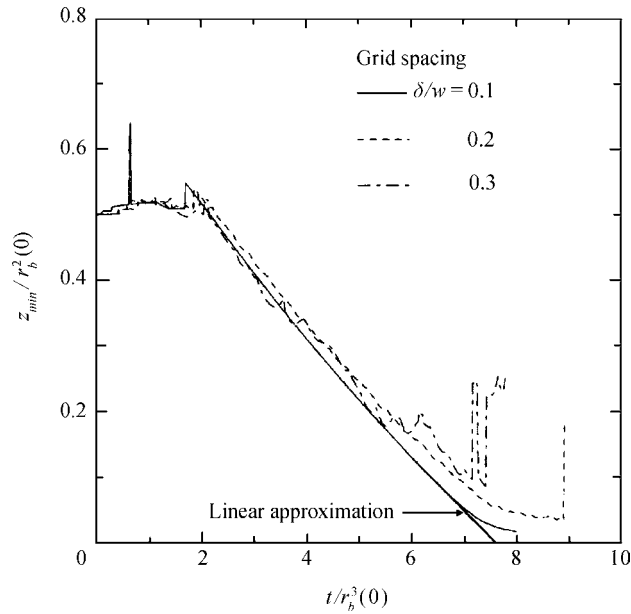


FIGURE 3. The minimum gap radius  $z_{min}/r_b^2(0)$  plotted against  $t/r_b^3(0)$ . The initial value of  $r_b$  is  $10^{-5}$  and the three resolutions correspond to the minimum distance between points in the tip region. The linear extrapolation gives  $t_{pinch} \simeq 7.6 r_b^3(0)$ .

present if two points come very close together, as happens at the tip. Indeed,  $\zeta$  increases by 1 between two successive points, whatever the distance between these two points.

At each time step, the Bernoulli equation and the kinematic condition were used to advance the solution using a Crank–Nicolson scheme (Press *et al.* 1992). The implicit equations were solved by iteration, which required less than 10 iterations for a relative error of  $10^{-5}$  in the velocity potential to be reached. An explicit Runge–Kutta fourth-order scheme was also tested, but found to be too unstable for small values of  $r_b$ .

We also redistribute grid points at every time step according to their distance from the tip. Cubic splines are used to interpolate to the new points. At each time step points are placed on the free surface with grid spacing  $\delta$ ; typical values are shown in figure 3. This spacing is used up to a distance of  $40r_b^2$  from the tip, after which it is gradually increased in steps of 2, since much lower resolution is required far from the tip.

#### 4. Reconnection

As we have explained above, the retraction of the meniscus is interrupted by the reconnection of the two sides of the gap, and the distance  $r_c$  by which the meniscus recoils as well as the time  $\tau_c$  required is given by the scaling relations (2.4). In figure 2 we define typical quantities characterizing the retraction of the meniscus. The minimum gap radius  $z_{min}$  marks the first trough of a train of capillary waves that is generated by the growing bubble. Note that in the corresponding simulation in Oguz & Prosperetti (1990), (cf. figure 4) there is little or no indication of this growth of capillary waves. We suspect that these authors did not follow the retraction for

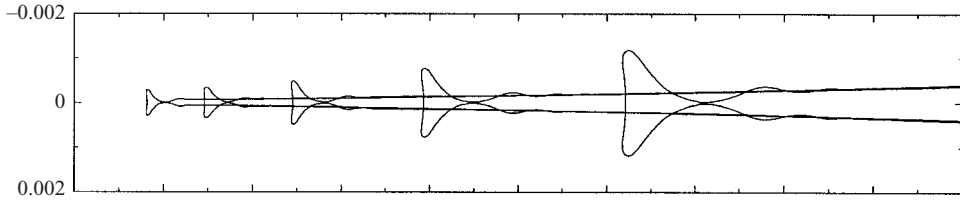


FIGURE 4. Successive entrainment of voids during the coalescence for an initial liquid bridge radius of  $r_b = 0.008$ . After every reconnection, the void is extracted from the profile and a new computation begins, with a null initial velocity field.

sufficiently long times, and that the low resolution of their simulation introduced additional damping, which smoothed out the capillary waves.

As seen in figure 3, the time dependence of the minimum gap radius  $z_{min}$  converges towards a close to linear behaviour as the resolution is increased. Extrapolation towards  $z_{min} = 0$  thus gives a reliable estimate of the time required for reconnection. Although the walls of the gap do not interact physically, errors of our boundary integral description grow large as two surfaces become close to each other. The reason is that the distance  $\lambda$  between points varies on scale  $z_{min}$  close to the minimum, so the grid spacing  $\delta$  always needs to be smaller than  $z_{min}$ .

From the simulations we deduce the values  $r_0 = 10$  and  $\tau_0 = 7.6$  for the reduced retraction length and time already reported in §2. Here the underlying assumption is that the dynamics is controlled by the local gap width alone. To test this idea, we have computed a sequence of pinch events as shown in figure 4. When  $z_{min}$  has reduced to about 10% of the local gap radius  $w/2$ , the gap is cut at about  $w/2$  behind the minimum and new points are introduced along the new surface. Our method of redistributing points automatically introduced a certain smoothing, which was enough for the simulation to continue. Obtaining a new initial condition for the velocity profile proved to be much more difficult. Simply extrapolating the velocity potential  $\varphi$  before the surgery to the new initial condition led to instabilities that could no longer be controlled numerically, so instead we had to put the velocity field to zero. This is justified by the fact that the gap position very quickly re-assumes its retraction velocity after the bubble is left behind, as we discuss in more detail below.

As illustrated in figure 4, this leads to a self-similar succession of pinch-off events. Each simulation was started from a new value of the bridge radius  $r_b^n$ . The typical gap width at the meniscus is then  $w = (r_b^n)^2$ . A more quantitative test of the scalings employed in §2 is presented in figure 5, where we plot the bridge radius  $r_b$  as a function of time and, in the inset,  $r_c/\tau_c = (r_0/\tau_0)/r_b^n$  as function of the bridge radius at the time of pinching. The excellent agreement with the predicted scaling behaviour confirms our assumption that the local dynamics only depends on the gap width at the corresponding radius  $r_b^n$ .

We did not follow the evolution of the bubble after it was cut off from the gap. Since it starts from a highly non-circular shape, it is expected to perform large-amplitude oscillations. Recalling that the bubble is really a torus in three-dimensional space, it will also be unstable with respect to the Rayleigh instability (Drazin & Reid 1982) and break up into a sequence of smaller bubbles. Evidently, this instability breaks the rotational symmetry and is thus well beyond the scope of the present work.

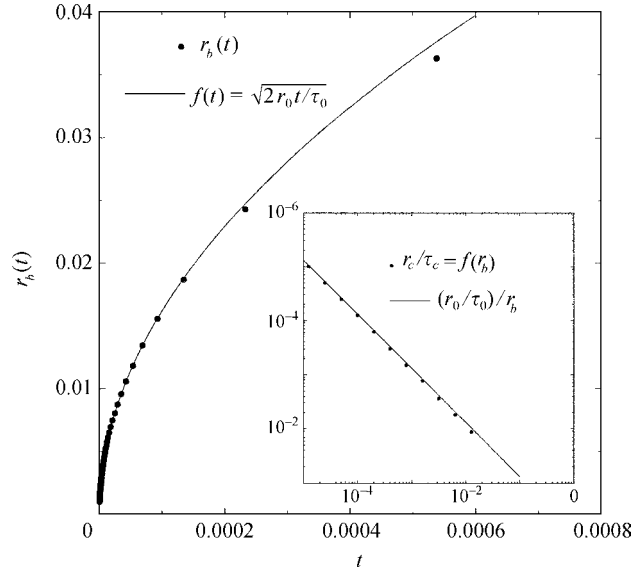


FIGURE 5. The minimum radius  $r_b$  as a function of time (dots), compared to the theoretical prediction  $\sqrt{2r_0t/\tau_0}$  (curve). Inset: the ratio  $r_c/\tau_c$  as a function of the initial radius  $r_b^0$  varying between  $1.25 \times 10^{-5}$  and  $1.28 \times 10^{-2}$ . The time for pinching  $\tau_c$  was approximated using a linear extrapolation of  $z_{min}$  (solid line). The numerical results show very good agreement with the expected scaling law.

## 5. Dynamics of retraction

We now study the individual retraction events, characterized by a mass of fluid being accelerated by two line forces, in greater detail. Thus if

$$\frac{dr_b}{dt} = v_{tip}$$

is the velocity of the receding tip, the force balance is

$$\frac{d}{dt} \left( M_{tip} \frac{dr_b}{dt} \right) = 2, \quad (5.1)$$

where  $M_{tip}$  is the mass being accelerated. This ‘added mass’ is being pushed along by the structure of maximum radius  $z_{max}$  that is forming at the end of the gap, and thus  $M_{tip} \approx Cz_{max}^2$  (Landau & Lifschitz 1982), where  $C$  is a numerical constant coming from the geometry of the void profile. Hence the equation of motion becomes

$$\frac{d}{dt} \left( Cz_{max}^2 \frac{dr_b}{dt} \right) = 2. \quad (5.2)$$

For short times, the bubble does not have time to grow, so  $z_{max}$  is approximately constant and given by the initial gap radius:  $z_{max} \approx r_b^0(0)/2$ . This corresponds to a constant mass being accelerated by a constant force, and (5.2) leads to a quadratic growth of the retraction distance:  $\delta r_b(t) = r_b(t) - r_b(0) \propto t^2$ . This is confirmed by the early time behaviour of  $\delta r_b(t)$  as shown in figure 6. Note that, consistent with (5.2),  $z_{max}$  remains constant.



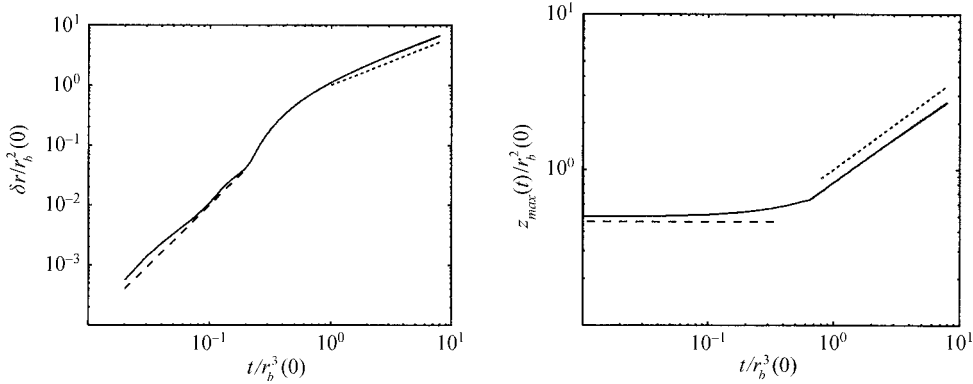


FIGURE 6. Two quantities characterizing retraction,  $\delta r = r_b(t) - r_b(0)$  and  $z_{max}$ , as functions of time in rescaled units. Dashed and dotted lines represent power-law approximations to the early and long-time behaviour, respectively. We find  $\delta r \propto t^{2 \pm 0.25}$  for early times, while  $z_{max}$  remains constant ( $\propto t^{\pm 0.05}$ ). For late times  $\delta r \propto t^{0.8 \pm 0.1}$  and  $z_{max} \propto t^{0.6 \pm 0.03}$ ; both behaviours are in agreement with (5.2).

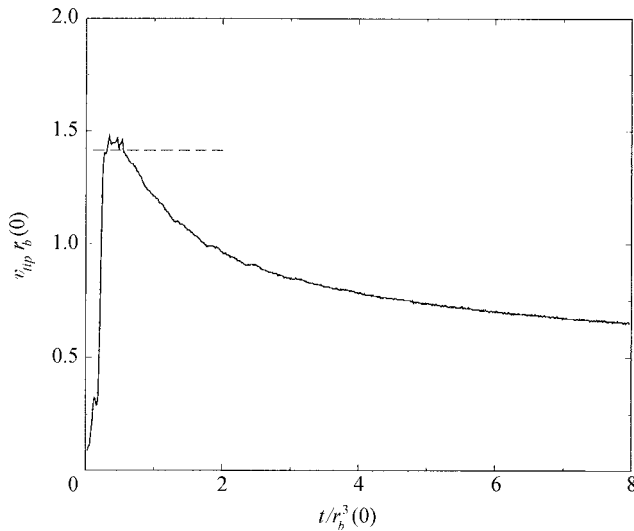


FIGURE 7. The speed of the retracting bridge  $v_{tip} = dr_b(t)/dt$  as a function of time in rescaled units. The Culick–Taylor velocity ( $\sqrt{2}$  in these units) is represented by the dashed line.

After this initial period of acceleration, the bubble radius  $z_{max}$  starts to grow and the speed of retraction  $v_{tip}$  reaches a maximum, as seen in figure 7. This maximum must be set by the initial width  $w$  of the gap, and thus dimensional arguments lead to

$$v_c \approx \sqrt{2/w}. \quad (5.3)$$

The prefactor in (5.3) comes from balancing the inertial term  $v_c^2/2$  with the surface tension force  $\kappa$  in (2.2), in analogy with the arguments of Culick and Taylor (Culick 1960; Taylor 1959) for receding soap films. The curvature  $\kappa$  has been approximated

by  $1/w$ . As confirmed by figure 7, the maximum of  $v_{tip}$  is approximated well by the estimate (5.3).

After reaching a maximum, the speed of retraction decreases steadily, as the bubble grows and with it the added mass that has to be dragged along. The transversal bubble expansion is due to the rapid fluid motion along its sides which, according to Bernoulli's equation (2.2), causes an under-pressure. Conversely, at the stagnation point behind the bubble the pressure is high and the bubble is curved inward (cf. figure 2). We do not yet have a fully quantitative theory of the bubble expansion, since this would require a precise knowledge of the bubble shape. Namely, the fluid speed  $v_m$  past the crest of the bubble is determined by its curvature  $\kappa_c$  (Lamb 1993):  $v_m = v_{tip}\kappa_c z_{max}$ , in analogy with the flow past an ellipsoidal body. To close the system of equations, we would need an expression for  $\kappa_c$ . However, we notice from figure 6 that the temporal growth of the bubble size  $z_{max}$  is described well by a power law:  $z_{max} \propto t^\alpha$  with  $\alpha = 0.6 \pm 0.03$ . Similarly we find  $\delta r_b \propto t^\beta$  with  $\beta = 0.8 \pm 0.1$ , in good agreement with equation (5.2). The range of validity of the power laws proposed here can of course never exceed an order of magnitude, since the gap pinches off after time  $t \approx 10r_b^3$ .

Eventually, when the toroidal bubble separates from the gap, the velocity  $v_{tip}$  has decreased to about half of  $v_c$ . Therefore, the effect of the dynamical pressure  $v_{tip}^2/2$  is reduced considerably relative to the capillary pressure. Numerically, we find that the capillary force is at least 4 times bigger than the dynamical pressure, which indicates that the velocity field can safely be neglected at reconnection, as we are forced to do owing to limitations of our numerical technique.

## 6. Discussion

We have shown that the merging of low-viscosity fluid droplets leads to a self-similar sequence of void entrancements. It is interesting to note that the same power law behaviour (2.6) of  $r_b$  can be formally derived from a continuous evolution if  $v_{tip}$  is assumed to be the Culick velocity (5.3). If the gap width  $w$  is estimated from the geometrical constraint  $w \approx r_b^2$ , this immediately leads to  $\partial_t r_b \approx \sqrt{2}/r_b$ , which can be integrated to give a power  $t^{1/2}$ . This is the argument given in Eggers *et al.* (1999), which did not take reconnection into account. The reason why it gives the correct answer (apart from the prefactor) is that the size of the gap tip is rescaled to agree with the geometrical estimate (2.3) at each reconnection event. Thus although the bubble actually grows to a much larger size than  $r_b^2$ , the balance implied by the above argument is actually true on average.

It might be equally tempting (J. R. Lister 2002, personal communication) to apply the same reasoning to the force balance (5.1), by approximating (at least on average) the added mass by  $M_{tip} \approx Cz_{max}^2 \propto r_b^4$ . Integrating the corresponding equation of motion leads to  $r_b \propto t^{2/5}$ . This apparent paradox is explained by the fact that the reconnection events destroy the momentum conservation implied by (5.1). Owing to bubble growth, momentum is distributed over a much larger volume than estimated from the simple geometrical argument. Accordingly, in the asymptotic limit of  $t \ll 1$  one obtains a motion that is faster than that given by the full calculation including reconnection.

We finally point out some questions inspired by this work. First, a more complete theory of the bubble growth at the end of the receding meniscus should be developed. Secondly, we are not yet able to fully treat the velocity field after reconnection. Such a treatment may lead to an increase in fluctuations and perhaps some randomness

during retraction. As pointed out in Oguz & Prosperetti (1990), a finite velocity of approach will increase the likelihood of bubble entrapment during coalescence. Other interesting generalizations not yet considered in the present paper are the effect of an external fluid as well as viscous corrections. Clearly, a number of theoretical questions remain open. Perhaps more importantly, detailed experimental studies are called for, for example to verify the phenomenon of bubble entrainment predicted by our analysis.

It is our pleasure to thank Stéphane Zaleski for his constant encouragement during this work.

## REFERENCES

- AMAROUCHE, A., CRISTOBAL, G. & KELLAY, H. 2001 Noncoalescing drops. *Phys. Rev. Lett.* **87**, art. no. 206104.
- BAKER, G. R., MEIRON, D. I. & ORSZAG, S. A. 1980 Vortex simulations of the rayleigh-taylor instability. *Phys. Fluids* **23**, 1485–1490.
- BRADLEY, S. G. & STOW, C. D. 1978 Collisions between liquid drops. *Phil. Trans. R. Soc. Lond. A* **287**, 635–675.
- CHAUDHARY, K. C. & MAXWORTHY, T. 1980 The nonlinear capillary instability of a liquid jet. Part 3. Experiments on satellite drops formation and control. *J. Fluid Mech.* **96**, 287–297.
- CROWDY, D. 2002 Exact solutions for the viscous sintering of multiply-connected fluid domains. *J. Engng Maths* **42**, 225–242.
- CROWDY, D. 2003 Viscous sintering of unimodal and bimodal cylindrical packings with shrinking pores. *Eur. J. Appl. Maths*. To appear.
- CULICK, F. E. C. 1960 Comments on a ruptured soap film. *J. Appl. Phys.* **31**, 1128.
- DRAZIN, P. G. & REID, W. H. 1982 *Hydrodynamic Stability*. Cambridge University Press.
- EGGERS, J. 1997 Nonlinear dynamics and breakup of free surface flows. *Rev. Mod. Phys.* **69**, 865–929.
- EGGERS, J. 1998 Coalescence of spheres by surface diffusion. *Phys. Rev. Lett.* **80**, 2634–2637.
- EGGERS, J., LISTER, J. R. & STONE, H. A. 1999 Coalescence of liquid drops. *J. Fluid Mech.* **401**, 293–310.
- FRENKEL, J. 1945 Viscous flow of crystalline bodies under the action of surface tension. *J. Phys. (Moscow)* **9**, 385–391.
- HOPPER, R. W. 1990 Plane stokes flow driven by capillarity on a free surface. *J. Fluid Mech.* **213**, 349–375.
- HOPPER, R. W. 1993 Coalescence of two viscous cylinders by capillarity: Part i. theory. *J. Am. Ceram. Soc.* **76**, 2947–2952.
- JURY, S. I., BLADON, P., KRISHNA, S. & CATES, M. E. 1999 Tests of dynamical scaling in three-dimensional spinodal decomposition. *Phys. Rev. E* **59**, R2535–R2538.
- LAFURIE, B., NARDONE, C., SCARDOVELLI, R., ZALESKI, S. & ZANETTI, G. 1994 Modelling merging and fragmentation in multiphase flows with surfer. *J. Comput. Phys.* **113**, 134–147.
- LAMB, H. 1993 *Hydrodynamics*. Cambridge University Press.
- LANDAU, L. D. & LIFSHITZ, E. M. 1982 *Fluid Mechanics*. Oxford University Press.
- MACPHEE, A. G., TATE, M. W., POWELL, F., YUE, Y., RENZI, M. J., ERCAN, A., NARAYANAN, S., FONTES, E., WALTHER, J., SCHALLER, J., GRUNER, S. M. & WANG, J. 2002 X-ray imaging of shock waves generated by high-pressure fuel sprays. *Science* **295**, 1261–1263.
- MARTINEZ-HERRERA, J. I. & DERBY, J. J. 1995 Viscous sintering of spherical particles via finite element analysis. *J. Am. Ceram. Soc.* **78**, 645–649.
- MENCHAGA-ROCHA, A., MARTNEZ-DVALOS, A., NEZ, R., POPINET, S. & ZALESKI, S. 2001 Coalescence of liquid drops by surface tension. *Phys. Rev. E* **63**, art. no. 046309.
- NIKOLAYEV, V. S., BEYSENS, D. & GUENOUN, P. 1996 New hydrodynamic mechanism for drop coarsening. *Phys. Rev. Lett.* **76**, 3144–3147.
- OGUZ, H. N. & PROSPERETTI, A. 1989 Surface-tension effects in the contact of liquid surfaces. *J. Fluid Mech.* **203**, 149–171.

- OGUZ, H. N. & PROSPERETTI, A. 1990 Bubble entrainment by the impact of drops on liquid surfaces. *J. Fluid Mech.* **219**, 143–179.
- PRESS, W. H., TEUKOLSKY, S. A., VETTERLING, W. T. & FLANNERY, B. P. 1992 *Numerical Recipes*. Cambridge University Press.
- RICHARDSON, S. 1992 Two-dimensional slow viscous flows with time-dependent free boundaries driven by surface tension. *Eur. J. Appl. Math* **3**, 193–207.
- TAYLOR, G. I. 1959 The dynamics of thin sheets of fluid. iii. disintegration of fluid sheets. *Proc. R. Soc. Lond. A* **253**, 313–321.
- VERDIER, C. 2000 Coalescence of polymer droplets: experiments on collision. *C. R. Acad. Sci. Paris IV* **1**, 119–126.
- WALLACE, D. B. 2001 Ink-jet applications, physics, and modelling – an industrial/applied research view. Presentation at IMA “Hot Topics” Workshop: Analysis and Modeling of Industrial Jetting Processes, <http://www.ima.umn.edu/multimedia/abstract/1-10abs.html#wallace>.
- YIANTOS, S. G. & DAVIS, R. H. 1991 Close approach and deformation of two viscous drops due to gravity and van der waals forces. *J. Colloid Interface Sci.* **144**, 412–433.